International Journal of Numerical Methods for Heat & Fluid ...

Heat and mass transfer in a porous medium filled rectangular duct with Soret and Dufour effects under inclined magnetic field

Ali J. Chamkha B. Mallikarjuna R. Bhuvana Vijaya D.R.V. Prasada Rao

Heat and mass transfer in a porous medium filled rectangular duct with Soret and Dufour effects under inclined magnetic field

Received 31 March 2013
Revised 15 June 2013
Accepted 7 August 2013

Ali J. Chamkha
Manufacturing Engineering Department, The Public Authority for Applied Education and Training, Shuweikh, Kuwait
B. Mallikarjuna and R. Bhuvana Vijaya
Mathematics Department, Jawaharlal Nehru Technological University Anantapur, Anantapur, India, and
D.R.V. Prasada Rao
Mathematics Department, Sri Krishnadevaraya University, Anantapur, India

Abstract

Purpose – The purpose of this paper is to study the effects of Soret and Dufour effects on convective heat and mass transfer flow through a porous medium in a rectangular duct in the presence of inclined magnetic field.

Design/methodology/approach – Using the non-dimensional variables, the governing equations have been transformed into a set of differential equations, which are non-linear and cannot be solved analytically, therefore finite element method has been used for solving the governing equations.

Findings – The influence of thermo-diffusion, diffusion thermo, radiation, dissipation, heat sources and the inclined magnetic field on all the flow, heat and mass transfer characteristics has been found to be significant.

Originality/value – The problem is relatively original as it combines many effects as Soret and Dufour effects and chemical reaction under inclined magnetic field.

Keywords Heat source, Heat and mass transfer, Soret and Dufour effects, Chemical reaction, Inclined magnetic field, Rectangular duct

Paper type Research paper

1. Introduction

The investigation of heat transfer in enclosures containing porous media began with experimental work of Verschoor and Greebler (1952). Verschoor and Greebler (1952) were followed by several other investigators interested in porous media heat transfer in rectangular enclosures (Ribando and Torrance, 1976; Rubin and Schweitzer, 1972; Seki *et al.*, 1981; Sivaiah, 2004). In particular, Bankvall (Bankvall, 1972, 1973, 1974) has published a great deal of practical work concerning heat transfer by natural convection in rectangular enclosures completely filled with porous media. Burns *et al.* (1926) have

One of the authors Mallikarjuna wishes to thank to the Department of Science and Technology, NewDelhi, India for providing financial support to enable conducting this research work under Inspire Program. The authors are very thankful to the editor and referees for their valuable comments and constructive suggestions which led to the improvement of the paper.

International Journal of Numerical Methods for Heat & Fluid Flow
Vol. 24 No. 7, 2014
pp. 1405-1436

0961-5539
DOI 10.1108/HFF-03-2013-0104

described a porous medium heat transfer flow in a rectangular geometry. Cheng and Hi (1987) have studied the flow and heat transfer rate in a rectangular box with solid walls using a Brinkman model the box is differentially heated in the horizontal direction. Chiu *et al.* (2007) have discussed mixed convection heat transfer in horizontal rectangular ducts with radiation effects. Chittibabu *et al.* (2006) has discussed convective flow in a porous rectangular duct with differential heated side wall using Brinkman model.

The convective heat and mass transfer occurs in a wide range of engineering and scientific fields such as oceanography, biology, chemical vapor transformation processes, pollution, astrophysics, geology and crystal growth techniques, for instance semi-conductors and alloys, where temperature and concentration differences are combined. Chamkha and Al-Naser (2002) investigated hydromagnetic double-diffusive convection in a rectangular enclosure with uniform side heat and mass fluxes and opposing temperature and concentration gradients. Other experimental studies dealing with thermo-solutal convection in rectangular enclosures were reported by Al-Farhany and Turan (2012) and Lee and Hyun (1990) and Hyun and Lee (1990).

Electrically conducting fluids in the presence of magnetic field have been applied extensively in various fields such as geothermal reservoir, metallurgical applications involving continuous casting and solidification of metal alloys and others and crystal growth. Magnetohydrodynamics is an academic discipline which studies the dynamics of electrically conducting fluids. Electromagnetic field has an important influence on the hydrodynamics. One of the main purposes of the electromagnetic control is to stabilize the flow and suppress oscillatory instabilities, which degrades the resulting crystal. Mahapatra *et al.* (2012) have studied mixed convection flow in an inclined enclosure under magnetic field with thermal radiation and heat generation. Magnetic field effect on the unsteady free convection flow in a square cavity filled with a porous medium with a constant heat generation reported by Revnic *et al.* (2011). Shehadeh and Duwairi (2009) investigated MHD natural convection in porous media-filled enclosures, which were in good agreement with, reported experimental results. Shanthi *et al.* (2011) have studied finite element analysis of convective heat and mass transfer flow of a viscous electrically conducting fluid through a porous medium in a rectangular cavity with dissipation. Nagaradhika *et al.* (2011) investigated convective heat transfer in a rectangular cavity under the influence of radiation, viscous dissipation and temperature gradient heat source.

In all these studies Soret and Dufour effects are assumed to be negligible. Such effects are significant when density differences exist in the flow regime. For instance, when heat and mass transfer occur simultaneously in a moving fluid, the relations between the fluxes and the driving potentials are of more intricate nature. Also, when species are introduced at a surface in fluid domain, with different (lower) density than the surrounding fluid, both Soret and Dufour effects can be significant. It has been found that an energy flux can be generated not only by temperature gradients but by composition gradients as well. The energy flux caused by a composition gradient is called the Dufour or diffusion-thermo effect. On the other hand, mass fluxes can also be created by temperature gradients and this is called the Soret or thermal-diffusion effect. The Soret effect, for example, has been utilized for isotope separation, and in mixture between gases with very light molecular weight (H_2, He) and of medium molecular weight (N_2, air), the Dufour effect was found to be of a considerable magnitude such that it cannot be ignored (Eckert and Drake, 1972). In view of these application (Gnaneswara Reddy and Bhaskar Reddy, 2010; Srinivas *et al.*, 2012;

Tai and Ming, 2010; Cheng, 2011; Dulal and Hiranmoy, 2011) have studied and reported the significance of Soret and Dufour effects.

Double diffusive natural convection problems with chemical reaction are of great importance in many processes and have received a considerable amount of attention in recent years. In particular all industrial chemical processes are designed to transform cheaper raw materials to high value products. A reactor, in which such chemical transformations take place, has to carry out several functions like bringing reactants into intimate contacts, providing an appropriate environment at adequate time, and allowing for the removal of products. Effect of chemical reaction and radiation absorption on the unsteady MHD free convection flow past a semi infinite vertical permeable moving plate with heat source and suction reported by Ibrahim *et al.* (2008). The effects of radiation absorption on MHD flow, heat and mass transfer problems have become more important in industrial area. At high operating temperature, radiation effect can be quite significant. Makinde (2005) examined the transient free convection interaction with thermal radiation of an absorbing-emitting fluid along moving vertical permeable plate. Rao and Shivaiah (2011) studied chemical reaction effects on unsteady MHD flow past semi-infinite vertical porous plate with viscous dissipation.

The objective of the present problem is to study the effects of Soret and Dufour effects on convective heat and mass transfer flow through a porous medium in a rectangular duct in the presence of inclined magnetic field. Using the non-dimensional variables, the governing equations have been transformed into a set of ordinary differential equations, which are non-linear and cannot be solved analytically, therefore finite element method has been used for solving it. The behaviors of the velocity, temperature, concentration, Nusselt number and Sherwood number are presented graphically for variations in the governing parameters.

2. Mathematical formulation

We consider the mixed convective heat and mass transfer flow of a viscous incompressible fluid in a saturated porous medium confined in the rectangular duct with internal heat sources (Figure 1) whose base length is a and height b. We assume that the enclosure is permeated by a uniform inclined magnetic field. The geometry and Cartesian coordinate system are schematically shown in Figure 1. Where the dimensional coordinates x and y are measures along the horizontal bottom wall and normal to it along the left vertical wall, respectively. The heat flux on the base and top

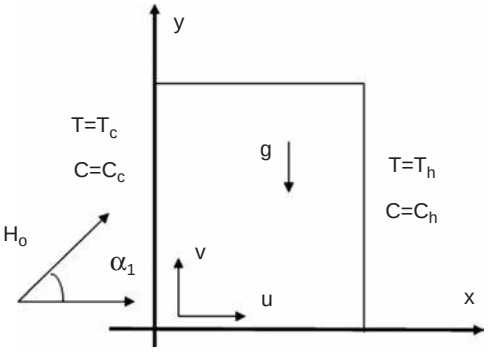

Figure 1.
Physical model

walls is maintained constant. The Cartesian coordinate system O(x,y) is chosen with origin on the central axis of the duct and its base parallel to x-axis.

We assume that:

(1) the convective fluid and the porous medium are everywhere in local thermodynamic equilibrium;

(2) there is no phase change of the fluid in the medium;

(3) the properties of the fluid and of the porous medium are homogeneous and isotropic;

(4) the porous medium is assumed to be closely packed so that Darcy's momentum law is adequate in the porous medium;

(5) the effect of buoyancy is included through well-known Boussinesq approximation; and

(6) the magnetic Reynolds number is assumed to be small so that the induced magnetic field can be neglected compared to the applied magnetic field.

Under these assumption the conservation equations for mass, Darcy, energy, diffusion and electric transfer along with the Boussinesq approximation are given by:

$$\frac{\partial u'}{\partial x'} + \frac{\partial v'}{\partial y'} = 0 \tag{1}$$

$$\frac{\partial u'}{\partial x'} - \frac{\partial v'}{\partial y'} = \frac{k}{\mu}\frac{\partial}{\partial x}(\rho' g) + \frac{\sigma \mu_e H_o^2}{\rho}\left(-\frac{\partial u'}{\partial y'} Sin^2(\gamma) + 2\frac{\partial v'}{\partial y'} Sin(\gamma) Cos(\gamma) + \frac{\partial v'}{\partial x} Cos^2(\gamma)\right) \tag{2}$$

$$\rho_\sigma c_p\left(u'\frac{\partial T}{\partial x'} + v'\frac{\partial T}{\partial y'}\right) = K_1\left(\frac{\partial^2 T}{\partial x'^2} + \frac{\partial^2 T}{\partial y'^2}\right) + Q + \left(\frac{\mu}{K}\right)(u^2 + v^2) - \frac{\partial (q_r)}{\partial x} + \frac{D_1 k T_1}{C_s C_p}\left(\frac{\partial^2 T}{\partial x'^2} + \frac{\partial^2 T}{\partial y'^2}\right) \tag{3}$$

$$\rho_\sigma c_p\left(u'\frac{\partial C}{\partial x'} + v'\frac{\partial C}{\partial y'}\right) = D_1\left(\frac{\partial^2 C}{\partial x'^2} + \frac{\partial^2 C}{\partial y'^2}\right) + \frac{D_1 k_T}{T_m}\left(\frac{\partial^2 T}{\partial x'^2} + \frac{\partial^2 T}{\partial y'^2}\right) - k'C \tag{4}$$

$$\rho' = \rho_0\{1 - \beta(T - T_0) - \beta^{\bullet}(C - C_0)\} \tag{5}$$

where:

$$T_0 = \frac{T_h + T_c}{2}, C_0 = \frac{C_h + C_c}{2}$$

and where u' and v' are Darcy velocities along x, y direction. T, C and g are the temperature, concentration and acceleration due to gravity. T_C, C_C and T_h, C_h are

the temperature and concentration on the cold and warm side walls, respectively. ρ, μ, ε and β are the density, coefficients of viscosity, kinematic viscosity and thermal expansion of the fluid, k is the permeability of the porous medium, K_1 is the cross diffusivity, β* is the volume coefficient of expansion with mass fraction concentration, q_r is the radiative heat flux and k_T is the thermal diffusion ratio, T_m is the mean fluid temperature and C_s is the concentration susceptibility.

The boundary conditions are:

$$\begin{aligned} &u' = v' = 0 && \text{on the boundary of the duct} \\ &T' = T_c, C = C_c && \text{on the side wall to the left} \\ &T' = T_h, C = C_h && \text{on the side wall to the right} \\ &\frac{\partial T'}{\partial y} = 0, \frac{\partial C}{\partial y} = 0 && \text{on the top (y = 0) and bottom} \\ &u = v = 0 && \text{walls (y = 0) which are insulated.} \end{aligned} \tag{6}$$

Invoking Rosseland approximation for radiation:

$$q_r = \frac{4\sigma^*}{3\beta_R}\frac{\partial T'^4}{\partial y}$$

Expanding T^4 in Taylor's series about T_e and neglecting higher order terms:

$$T'^4 \cong 4T_e^3 T - 3T_e^4$$

We now introduce the following non-dimensional variables:

$$\begin{aligned} &x' = ax; && y' = by; && c = b/a \\ &u' = (v/a)\,u; && v' = (v/a)\,u; && p' = \left(v^2\rho/a^2\right) p \\ &T = T_0 + \theta(T_h - T_c) && C = C_0 + \phi(C_h - C_c) \end{aligned} \tag{7}$$

The governing equations in the non-dimensional form are:

$$\frac{\partial u}{\partial x} - \frac{\partial v}{\partial y} = Ra\left(\frac{\partial \theta}{\partial x} + N\frac{\partial \phi}{\partial x}\right) + M^2\left(-\frac{\partial u'}{\partial y}Sin^2(\gamma) + 2\frac{\partial v'}{\partial y}Sin(\gamma)Cos(\gamma) + \frac{\partial v' Cos^2(\gamma)}{\partial x}\right) \tag{8}$$

$$P\left(u\frac{\partial \theta}{\partial x} + v\frac{\partial \theta}{\partial y}\right) = \left(1 + \frac{4N}{3}\right)\left(\frac{\partial^2 \theta}{\partial x^2} + \frac{\partial^2 \theta}{\partial y^2}\right) + \alpha + E_C\left(u^2 + v^2\right) + DuP\left(\frac{\partial^2 \phi}{\partial x^2} + \frac{\partial^2 \phi}{\partial y^2}\right) \tag{9}$$

$$Sc\left(u\frac{\partial \phi}{\partial x} + v\frac{\partial \phi}{\partial y}\right) = \left(\frac{\partial^2 \phi}{\partial x^2} + \frac{\partial^2 \phi}{\partial y^2}\right) + ScSo\left(\frac{\partial^2 \theta}{\partial x^2} + \frac{\partial^2 \theta}{\partial y^2}\right) - k\phi \tag{10}$$

In view of the equation of continuity we introduce the stream function ψ as:

$$u = \frac{\partial \psi}{\partial y}; \quad v = -\frac{\partial \psi}{\partial x} \tag{11}$$

Eliminating the pressure p from the Equation (9) and (10) and making use of (11) the equations in terms of ψ and θ are:

$$\nabla^2 \psi = -Ra\left(\frac{\partial \theta}{\partial x} + N\frac{\partial \phi}{\partial x}\right) + M^2\left(\frac{\partial^2 \psi}{\partial y^2} Sin^2\gamma + 2\frac{\partial^2 \psi}{\partial x \partial y} Sin(\gamma)Cos(\gamma) + \frac{\partial^2 \psi}{\partial x^2} Cos^2(\gamma)\right) \tag{12}$$

$$P\left(\frac{\partial \psi}{\partial y}\frac{\partial \theta}{\partial x} - \frac{\partial \psi}{\partial x}\frac{\partial \theta}{\partial y}\right) = \left(1 + \frac{4}{3N_1}\right)\left(\frac{\partial^2 \theta}{\partial x^2} + \frac{\partial^2 \theta}{\partial y^2}\right) - \alpha\theta + E_C\left(\left(\frac{\partial \psi}{\partial y}\right)^2 + \left(\frac{\partial \psi}{\partial x}\right)^2\right) + Du\ P\left(\frac{\partial^2 \phi}{\partial x^2} + \frac{\partial^2 \phi}{\partial y^2}\right) \tag{13}$$

$$Sc\left(\frac{\partial \psi}{\partial y}\frac{\partial \phi}{\partial x} - \frac{\partial \psi}{\partial x}\frac{\partial \phi}{\partial y}\right) = \left(\frac{\partial^2 \phi}{\partial x^2} + \frac{\partial^2 \phi}{\partial y^2}\right) + ScSo\left(\frac{\partial^2 \theta}{\partial x^2} + \frac{\partial^2 \theta}{\partial y^2}\right) - k\phi \tag{14}$$

where:

$$G = \frac{g\beta(T_h - T_c)a^3}{v^2} \quad \text{(Grashof number)}$$

$$M^2 = \frac{\sigma \mu_e^2 H_o^2 L^2}{v^2} \quad \text{(Hartmann number)}$$

$$P = \mu\, c_p / K_1 \quad \text{(Prandtl number)}$$

$$\alpha = Qa^z/(T_h - T_c)k_1 \quad \text{(Heat source parameter)}$$

$$Ra = \frac{\beta g(T_g - T_c)Ka}{v^2} \quad \text{(Rayleigh Number)}$$

$$N_1 = \frac{3\beta_R K_1}{4\sigma^{\bullet} : T_e^3} \quad \text{(Radiation parameter)}$$

$$Sc = \frac{v}{D_1} \quad \text{(Schmidt Number)}$$

$$So = \frac{D_1 k_T \Delta T}{\nu T_m \Delta C} \quad \text{(Soret parameter)}$$

$$Du = \frac{D_1 k_T \Delta C}{C_s C_p \nu \Delta T} \quad \text{(Dufour number)}$$

$$N = \frac{\beta^*(C_h - C_c)}{\beta(T_h - T_c)} \quad \text{(Buoyancy ratio)}$$

$$Ec = \left(\frac{a^4}{\mu K K_1 \Delta T}\right) \quad \text{(Eckert number)}$$

$$k = \frac{KL^2}{D_1} \quad \text{(Chemical reaction parameter)}$$

The boundary conditions are:

$$\frac{\partial \psi}{\partial x} = 0, \frac{\partial \psi}{\partial y} = 0 \; on \; x = 0 \; \& \; 1 \tag{15}$$

$$\begin{aligned} \theta &= 1 \; \phi = 1 \; on \; x = 0 \\ \theta &= 0 \; \phi = 0 \; on \; x = 1 \end{aligned} \tag{16}$$

3. Method of solution

Finite element analysis

The set of differential equations given in (12)-(14) is highly non-linear and therefore, cannot be solved analytically. Hence finite element method has been used for solving it. The finite element method is powerful technique for solving ordinary and partial differential equations. This method is so general that it can be applied to a wide variety of engineering problems including heat transfer, fluid mechanics, solid mechanics and chemical processing. For the finite element method one can refer to Bathe (1996) and Reddy (1985).

The region is divided into a finite number of three node triangular elements, in each of which the element equation is derived using Galerkin weighted residual method. In each element f_i the approximate solution for an unknown f in the variational formulation is expressed as a linear combination of shape function. N_k^i, $k = 1,2,3$, which are linear polynomials in x and y. This approximate solution of the unknown f coincides with actual values at each node of the element. The variational formulation results in a 3×3 matrix equation (stiffness matrix) for the unknown local nodal values of the given element. These stiffness matrices are assembled in terms of global nodal values using inter element continuity and boundary conditions resulting in global matrix equation.

In each case there are r distinct global nodes in the finite element domain and f_p, $p = 1,2, \ldots, r$ is the global nodal values of any unknown f defined over the domain then:

$$f = \sum_{i=1}^{8} \sum_{p=1}^{r} f_p \, \Phi_{\mathrm{p}}^{\mathrm{i}},$$

where the first summation denotes summation over s elements and the second one represents summation over the independent global nodes and $\Phi_p^i = N_N^i$, if p is one of the local nodes say k of the element $e_i = 0$, otherwise. f_p's are determined from the global matrix equation. Based on these lines we now make a finite element analysis of the given problem governed by (12)-(14) subjected to the conditions (15)-(16).

Let ψ^i, θ^i and ϕ^i be the approximate values of ψ, θ and ϕ:

$$\psi^i = N_1^i \psi_1^i + N_2^i \psi_2^i + N_3^i \psi_3^i \tag{17a}$$

$$\theta^i = N_1^i \theta_1^i + N_2^i \theta_2^i + N_3^i \theta_3^i \tag{17b}$$

$$\phi = N_1^i \phi_1^i + N_2^i \phi_2^i + N_3^i \phi_3^i \tag{17c}$$

Substituting the approximate value ψ^i, θ^i and ϕ^i for ψ, θ and ϕ, respectively in (13), the error:

$$\begin{aligned} E_1^i = & \left(1 + \frac{4}{3N_1}\right) \frac{\partial^2 \theta^i}{\partial x^2} + \frac{\partial^2 \theta^i}{\partial y^2} - P\left(\frac{\partial \psi^i}{\partial y} \frac{\partial \theta^i}{\partial x} - \frac{\partial \psi^i}{\partial x} \frac{\partial \theta^i}{\partial y}\right) + \alpha \\ & + E_C \left[\left(\frac{\partial \psi}{\partial y}\right)^2 + \left(\frac{\partial \psi}{\partial x}\right)^2\right] + DuP\left(\frac{\partial^2 \phi^i}{\partial x^2} + \frac{\partial^2 \phi^i}{\partial y^2}\right) \end{aligned} \tag{18}$$

$$E_2^i = \frac{\partial^2 \phi^i}{\partial x^2} + \frac{\partial^2 \phi^i}{\partial y^2} - Sc\left(\frac{\partial \psi^i}{\partial y} \frac{\partial \phi^i}{\partial x} - \frac{\partial \psi^i}{\partial x} \frac{\partial \phi^i}{\partial y}\right) + ScSo\left(\frac{\partial^2 \theta^i}{\partial x^2} + \frac{\partial^2 \theta^i}{\partial y^2}\right) - k\phi^i \tag{19}$$

Under Galerkin method this error is made orthogonal over the domain of e_i to the respective shape functions (weight functions) where:

$$\int_{ei} E_1^i N_k^i d\Omega = 0,$$

$$\int_{ei} E_2^i N_k^i d\Omega = 0$$

$$\int_{ei=} N_k^i \left(\left(1+\frac{4}{3N_1}\right)\left(\frac{\partial^z\theta^i}{\partial x^2}+\frac{\partial^z\theta^i}{\partial y^2}\right) - P\left(\frac{\partial\psi^i}{\partial y}\frac{\partial\theta^i}{\partial x}-\frac{\partial\psi^i}{\partial x}\frac{\partial\theta^i}{\partial y}\right) + \alpha + \left[E_C\left(\frac{\partial\psi}{\partial y}\right)^2+\left(\frac{\partial\psi}{\partial x}\right)^2\right] + DuP\left(\frac{\partial^2\phi^i}{\partial x^2}+\frac{\partial^2\phi^i}{\partial y^2}\right)\right) d\Omega = 0 \tag{20}$$

$$\int_{ei=} N_k^i \left(\left(\frac{\partial^z\phi^i}{\partial x^2}+\frac{\partial^z\phi^i}{\partial y^2}\right) - Sc\left(\frac{\partial\psi^i}{\partial y}\frac{\partial\phi^i}{\partial x}-\frac{\partial\psi^i}{\partial x}\frac{\partial\phi^i}{\partial y}\right) + ScSo\left(\frac{\partial^z\theta^i}{\partial x^2}+\frac{\partial^z\theta^i}{\partial y^2}\right) - k\phi^i\right) d\Omega = 0 \tag{21}$$

Using Green's theorem we reduce the surface integral (20) and (21) without affecting ψ terms and obtain:

$$\int_{ei} N_k^i \left\{ \begin{array}{l} \left(1+\frac{4}{3N_1}\right)\frac{\partial N_k^i}{\partial x}\frac{\partial\theta^i}{\partial x}+\frac{\partial N_k^i}{\partial y}\frac{\partial\theta^i}{\partial y} - PN_k\left(\frac{\partial\psi^i}{\partial y}\frac{\partial\theta^i}{\partial x}-\frac{\partial\psi^i}{\partial x}\frac{\partial\theta^i}{\partial y}\right) \\ +\alpha + E_C\left(\frac{\partial\psi}{\partial y}\right)^2+\left(\frac{\partial\psi}{\partial x}\right)^2 \end{array} \right\} d\Omega = \int_{\Gamma i} N_k^i \left(\frac{\partial\theta^i}{\partial x}n_x+\frac{\partial\theta^i}{\partial y}n_y\right) d\Gamma_i \tag{22}$$

$$\int_{eiei} N_k^i \left\{ \begin{array}{l} \frac{\partial N_k^i}{\partial x}\frac{\partial\phi^i}{\partial x}+\frac{\partial N_k^i}{\partial y}\frac{\partial\phi^i}{\partial y} - Sc^i N_k\left(\frac{\partial\psi^i}{\partial y}\frac{\partial\phi^i}{\partial x}-\frac{\partial\psi^i}{\partial x}\frac{\partial\phi^i}{\partial y}\right) \\ +ScSo\left(\frac{\partial N_k^i}{\partial x}\frac{\partial\theta^i}{\partial x}+\frac{\partial N_k^i}{\partial y}\frac{\partial\theta^i}{\partial y}\right) - k\int_{ei}\phi^i N_k^i d\Omega \end{array} \right\} d\Omega = \int_{\Gamma i} N_k^i \left(\frac{\partial\theta^i}{\partial x}+\frac{ScSo}{N}\frac{\partial\phi^i}{\partial x}\right)n_x + \left(\frac{\partial\theta^i}{\partial y}+ScSo\frac{\partial\theta^i}{\partial y}n_y\right) d\Gamma_i \tag{23}$$

where Γ_I is the boundary of e_i.

Substituting LHS of (17a)-(17c) for ψ^i, θ^i and ϕ^i in (22) and (23) we get:

$$\sum_1 \int_{ei} \left(1+\frac{4N}{3}\right)\frac{\partial N_k^i}{\partial x}\frac{\partial N_L^i}{\partial x}+\frac{\partial N_k^i}{\partial y}\frac{\partial N_L^i}{\partial y} - P\sum_1 \psi_m^i \int_{ei}\left(\frac{\partial N_m^i}{\partial y}\frac{\partial N_L^i}{\partial x}-\frac{\partial N_m^i}{\partial x}\frac{\partial N_L^i}{\partial y}\right) d\Omega + \alpha\int_{ei} N_k^i d\Omega + E_C\int_{ei}\left(\left(\frac{\partial\psi}{\partial y}\right)^2+\left(\frac{\partial\psi}{\partial x}\right)^2\right) + DuP\sum_1\int_{ei}\phi^i\left(\frac{\partial N_k^i}{\partial x}\frac{\partial N_L^i}{\partial x}+\frac{\partial N_L^i}{\partial y}\frac{\partial N_k^i}{\partial y}\right) d\Omega = \int_{\Gamma_i} N_k^i\left(\frac{\partial\theta^i}{\partial x}n_x+\frac{\partial\theta^i}{\partial y}n_y\right) d\Gamma_i = Q_k^i \qquad (l,m,k=1,2,3) \tag{24}$$

$$\sum_{1}\int_{ei}\phi^{i}\left(\frac{\partial N_k^i}{\partial x}\frac{\partial N_L^i}{\partial x}+\frac{\partial N_L^i}{\partial y}\frac{\partial N_k^i}{\partial y}\right)-Sc\sum_{1}\psi_m^i\int_{ei}\left(\frac{\partial N_m^i}{\partial y}\frac{\partial N_L^i}{\partial x}-\frac{\partial N_m^i}{\partial x}\frac{\partial N_L^i}{\partial y}\right)d\Omega$$

$$+ScSo\sum\theta^i\int_{ei}\left(\frac{\partial N_k^i}{\partial x}\frac{\partial N_L^i}{\partial x}+\frac{\partial N_L^i}{\partial y}\frac{\partial N_k^i}{\partial y}\right)d\Omega_i-k\sum_{1}\int_{ei}\phi^i N_k^i N_L^i d\Omega_i$$

$$=\int_{\Gamma i}N_k^i\left(\frac{\partial\theta^i}{\partial x}+ScSo\frac{\partial\theta^i}{\partial x}\right)n_x+\left(\frac{\partial\theta^i}{\partial y}+ScSo\frac{\partial\theta^i}{\partial y}n_y\right)d\Gamma_i=Q_i^C\qquad(l,m,k=1,2,3) \tag{25}$$

where $Q_k^i=Q_{k1}^i+Q_{k2}^i+Q_{k3}^i$, Q_k^i's being the values of Q_k^i on the sides s = (1,2,3) of the element e_i. The sign of Q_k^i's depends on the direction of the outward normal w.r.t the element.

Choosing different N_k^i's as weight functions and following the same procedure we obtain matrix equations for three unknowns (Q_p^i) viz.:

$$(a_p^i)(\theta_p^i)=(Q_k^i) \tag{26}$$

where (a_{pk}^i) is a 3 × 3 matrix, $(\theta^i{}_p)$,(Q_k^i) are column matrices.

Repeating the above process with each of s elements, we obtain sets of such matrix equations. Introducing the global coordinates and global values for θ_p^i and making use of inter element continuity and boundary conditions relevant to the problem the above stiffness matrices are assembled to obtain a global matrix equation. This global matrix is r × r square matrix if there are r distinct global nodes in the domain of flow considered.

Similarly substituting ψ^i, θ^i and ϕ^i in (12) and defining the error:

$$E_3^i=\nabla^2\psi+\mathrm{Ra}\left(\frac{\partial\theta}{\partial \mathrm{x}}+N\frac{\partial\phi}{\partial \mathrm{x}}\right)-M^2\left(\frac{\partial^2\psi}{\partial y^2}Sin^2\gamma+2\frac{\partial^2\psi}{\partial x\partial y}Sin(\gamma)Cos(\gamma)+\frac{\partial^2\psi}{\partial x^2}Cos^2(\gamma)\right)$$

$$=\left(1+M^2Cos^2(\gamma)\frac{\partial^2\psi}{\partial x^2}\right)+\left(1+M^2Sin^2(\gamma)\frac{\partial^2\psi}{\partial y^2}+2M^2Sin(\gamma)Cos(\gamma)\frac{\partial^2\psi}{\partial x\partial y}\right.$$

$$\left.+\mathrm{Ra}\left(\frac{\partial\theta}{\partial \mathrm{x}}+N\frac{\partial\phi}{\partial \mathrm{x}}\right)\right. \tag{27}$$

and following the Galerkin method we obtain:

$$\int_{\Omega}E_3^i\psi_j^i d\Omega=0 \tag{28}$$

Using Green's theorem (3.8) reduces to:

$$\int_{\Omega}\left(\begin{array}{l}(1+M^2Cos^2(\gamma))\frac{\partial N_k^i}{\partial x}\frac{\partial \psi^i}{\partial x}+(1+M^2Sin^2(\gamma))\frac{\partial N_k^i}{\partial y}\frac{\partial \psi^i}{\partial y}\\+2M^2Sin(\gamma)Cos(\gamma)\frac{\partial N_k^i}{\partial y}\frac{\partial \psi^i}{\partial y}+\mathrm{Ra}(\theta^i\frac{\partial N_k^i}{\partial x}+\phi^i\frac{\partial N_k^i}{\partial x})\end{array}\right)d\Omega$$
$$=\int_{\Gamma}N_k^i\left(\frac{\partial \psi^i}{\partial x}n_x+\frac{\partial \psi^i}{\partial y}n_y\right)d\Gamma_i+\int_{\Gamma}N_k^i n_x\theta^i d\Gamma_i \tag{29}$$

In obtaining (29) the Green's theorem is applied w.r.t derivatives of ψ without affecting θ terms.

Using (17) and (18) in (29) we have:

$$\sum_m \psi_m^i\left\{\begin{array}{l}\int_{\Omega}(1+M^2Cos^2(\gamma))\left(\begin{array}{l}\frac{\partial N_k^i}{\partial x}\frac{\partial N_m^i}{\partial x}+(1+M^2Sin^2(\gamma))\frac{\partial N_m^i}{\partial y}\frac{\partial N_k^i}{\partial y}\\+2M^2Sin(\gamma)Cos(\gamma)\frac{\partial N_k^i}{\partial y}\frac{\partial \psi^i}{\partial y}\end{array}\right)d\Omega_i\\+\mathrm{Ra}\sum_L(\theta_L^i\int_{\Omega i}N_k^i\frac{\partial N_L^i}{\partial x}d\Omega+\phi_L^i N\int_{\Omega i}\mathrm{N_k^i}\frac{\partial N_L^i}{\partial x}d\Omega\end{array}\right\}$$
$$=\int_{\Gamma}N_k^i\left(\frac{\partial \psi^i}{\partial x}n_x+\frac{\partial \psi^i}{\partial y}n_y\right)d\Gamma_i+\int_{\Gamma}N_k^i\theta^i d\Omega_i=\Gamma_k^i \tag{30}$$

In the problem under consideration, for computational purpose, we choose uniform mesh of ten triangular element (Figure 2). The domain has vertices whose global coordinates are (0,0), (1,0) and (1,c) in the non-dimensional form. Let $e_1, e_2, \ldots, e_{10}$ be the ten elements and let $\theta_1, \theta_2, \ldots, \theta_{10}$ be the global values of θ and $\psi_1, \psi_2, \ldots, \psi_{10}$ be the global values of ψ at the ten global nodes of the domain (Figure 2).

4. Shape functions and stiffness matrices

Range functions in $\underset{i,j}{n}$; i = element, j = node:

$$\underset{1,1}{n}=1-3x \qquad \underset{1,2}{n}=3x-\frac{3y}{C}$$

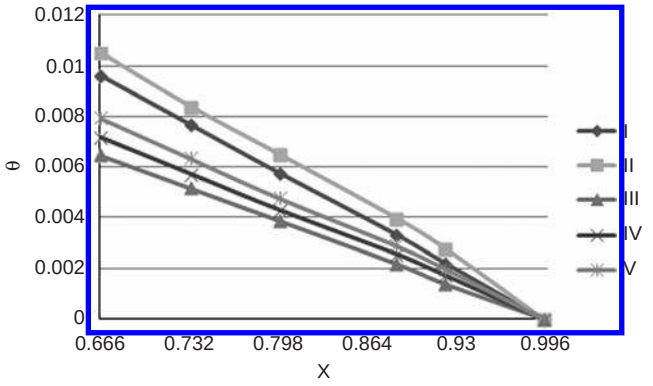

Figure 2.
Variation of θ with So at y = c/3 level

$$\underset{2,1}{n} = 1 - \frac{3y}{C} \qquad \underset{2,2}{n} = -1 + \frac{3y}{C}$$

$$\underset{2,3}{n} = 1 - 3x + \frac{3y}{C} \qquad \underset{3,1}{n} = 2 - 3x$$

$$\underset{3,2}{n} = -1 + 3x - \frac{3y}{C} \qquad \underset{3,3}{n} = \frac{3y}{C}$$

$$\underset{4,1}{n} = 1 - \frac{3y}{C} \qquad \underset{4,2}{n} = -2 + 3x$$

$$\underset{4,3}{n} = 2 - 3x + \frac{3y}{C} \qquad \underset{5,1}{n} = 2 - 3x$$

$$\underset{5,2}{n} = -1 + 3x - \frac{3y}{C} \qquad \underset{5,3}{n} = \frac{3y}{C}$$

$$\underset{6,1}{n} = 2 - 3x \qquad \underset{6,2}{n} = 3x - \frac{3y}{C}$$

$$\underset{6,3}{n} = 1 + \frac{3y}{C} \qquad \underset{7,1}{n} = 2 - \frac{3y}{C}$$

$$\underset{7,2}{n} = -2 + 3x \qquad \underset{7,3}{n} = 1 - 3x + \frac{3y}{C}$$

$$\underset{8,1}{n} = 3 - 3x \qquad \underset{8,2}{n} = -1 + 3x - \frac{3y}{C}$$

$$\underset{9,2}{n} = 3x - \frac{3y}{C} \qquad \underset{9,3}{n} = -1 + \frac{3y}{C}$$

Substituting the above shape functions in (24), (25) and (30) w.r.t each element and integrating over the respective triangular domain we obtain the element in the form (24). The 3×3 matrix equations are assembled using connectivity conditions to obtain a 8×8 matrix equations for the global nodes ψ_p,θ_p and ϕ_p.

The global matrix equation for θ is:

$$A_3 X_3 = B_3 \tag{31}$$

The global matrix equation for ϕ is

$$A_4 X_4 = B_4 \tag{32}$$

The global matrix equation for ψ is

$$A_5 X_5 = B_5 \tag{33}$$

where:

$$A_3 = \begin{pmatrix} -1 & a_{12} & a_{13} & 0 & 0 & 0 & 0 & 0 & 0 & 0 & 0 \\ 0 & a_{22} & a_{23} & 0 & 0 & 0 & 0 & 0 & 0 & 0 & 0 \\ 0 & a_{32} & a_{33} & a_{34} & a_{35} & 0 & 0 & 0 & 0 & 0 & 0 \\ 0 & 0 & a_{44} & a_{44} & a_{45} & 0 & 0 & 0 & 0 & 0 & 0 \\ 0 & 0 & a_{53} & a_{54} & a_{55} & a_{56} & a_{57} & 0 & 0 & 0 & 0 \\ 0 & 0 & 0 & 0 & a_{65} & a_{66} & a_{67} & 0 & 0 & 0 & 0 \\ 0 & 0 & 0 & 0 & a_{75} & a_{76} & a_{77} & a_{78} & a_{79} & 0 & 0 \\ 0 & 0 & 0 & 0 & 0 & 0 & a_{87} & a_{88} & a_{89} & 0 & 0 \\ 0 & 0 & 0 & 0 & 0 & 0 & a_{97} & a_{98} & a_{99} & a_{910} & 0 \\ 0 & 0 & 0 & 0 & 0 & 0 & 0 & 0 & a_{109} & a_{1010} & 0 \\ 0 & 0 & 0 & 0 & 0 & 0 & 0 & 0 & a_{119} & a_{1110} & -1 \end{pmatrix}$$

$$A_4 = \begin{pmatrix} 1 & b_{1,2} & b_{1,3} & 0 & 0 & 0 & 0 & 0 & 0 & 0 & 0 \\ 0 & b_{2,2} & b_{2,3} & 0 & 0 & 0 & 0 & 0 & 0 & 0 & 0 \\ 0 & b_{3,2} & b_{3,3} & b_{3,4} & b_{3,5} & 0 & 0 & 0 & 0 & 0 & 0 \\ 0 & 0 & b_{4,3} & b_{4,4} & b_{4,5} & 0 & 0 & 0 & 0 & 0 & 0 \\ 0 & 0 & b_{5,3} & b_{5,4} & b_{5,5} & b_{5,6} & b_{5,7} & 0 & 0 & 0 & 0 \\ 0 & 0 & 0 & 0 & b_{6,5} & b_{6,6} & b_{6,7} & 0 & 0 & 0 & 0 \\ 0 & 0 & 0 & 0 & b_{7,5} & b_{7,6} & b_{7,7} & b_{7,8} & b_{7,9} & 0 & 0 \\ 0 & 0 & 0 & 0 & 0 & 0 & b_{8,7} & b_{8,8} & b_{8,9} & 0 & 0 \\ 0 & 0 & 0 & 0 & 0 & 0 & b_{9,7} & b_{9,8} & b_{9,9} & b_{9,10} & 0 \\ 0 & 0 & 0 & 0 & 0 & 0 & 0 & 0 & b_{10,9} & b_{10,10} & 0 \\ 0 & 0 & 0 & 0 & 0 & 0 & 0 & 0 & b_{11,9} & b_{11,10} & b_{11,11} \end{pmatrix}$$

$$A_5 = \begin{pmatrix} -1 & 0 & 0 & 0 & 0 & 0 & 0 & 0 & 0 & 0 \\ 0 & -1 & 0 & 0 & 0 & 0 & 0 & 0 & 0 & 0 \\ 0 & 0 & -1 & 0 & 0 & 0 & 0 & 0 & 0 & 0 \\ 0 & 0 & 0 & -1 & 0 & 0 & 0 & 0 & 0 & 0 \\ 0 & 0 & 0 & 0 & -1 & 0 & 0 & 0 & 0 & 0 \\ 0 & 0 & 0 & 0 & 0 & 0 & 0 & 0 & 0 & 0 \\ 0 & 0 & 0 & 0 & 0 & 0 & 0 & 0 & 0 & 0 \\ 0 & 0 & 0 & 0 & 0 & 0 & 0 & 0 & 0 & 0 \\ 0 & 0 & 0 & 0 & 0 & 0 & 0 & 0 & -1 & 0 \\ 0 & 0 & 0 & 0 & 0 & 0 & 0 & 0 & 0 & -1 \end{pmatrix}$$

$$X_3 = \begin{bmatrix} \theta_1 \\ \theta_2 \\ \theta_3 \\ \theta_4 \\ \theta_5 \\ \theta_6 \\ \theta_7 \\ \theta_8 \\ \theta_9 \\ \theta_{10} \\ \theta_{11} \end{bmatrix} \qquad X_4 = \begin{bmatrix} C_1 \\ C_2 \\ C_3 \\ C_4 \\ C_5 \\ C_6 \\ C_7 \\ C_8 \\ C_9 \\ C_{10} \\ C_{11} \end{bmatrix} \qquad X_5 = \begin{bmatrix} u_1 \\ u_2 \\ u_3 \\ u_4 \\ u_5 \\ u_6 \\ u_7 \\ u_8 \\ u_9 \\ u_{10} \\ u_{11} \end{bmatrix}$$

$$\mathrm{B}_3 = \begin{bmatrix} \mathrm{ar}_1 \\ \mathrm{ar}_2 \\ \mathrm{ar}_3 \\ \mathrm{ar}_4 \\ \mathrm{ar}_5 \\ \mathrm{ar}_6 \\ \mathrm{ar}_7 \\ \mathrm{ar}_8 \\ \mathrm{ar}_9 \\ \mathrm{ar}_{10} \\ \mathrm{ar}_{11} \end{bmatrix} \qquad \mathrm{B}_4 = \begin{bmatrix} \mathrm{br}_1 \\ \mathrm{br}_2 \\ \mathrm{br}_3 \\ \mathrm{br}_4 \\ \mathrm{br}_5 \\ \mathrm{br}_6 \\ \mathrm{br}_7 \\ \mathrm{br}_8 \\ \mathrm{br}_9 \\ \mathrm{br}_{10} \\ \mathrm{br}_{11} \end{bmatrix} \qquad \mathrm{B}_5 = \begin{bmatrix} \mathrm{cr}_1 \\ \mathrm{cr}_2 \\ \mathrm{cr}_3 \\ \mathrm{cr}_4 \\ \mathrm{cr}_5 \\ \mathrm{cr}_6 \\ \mathrm{cr}_7 \\ \mathrm{cr}_8 \\ \mathrm{cr}_9 \\ \mathrm{cr}_{10} \\ \mathrm{cr}_{11} \end{bmatrix}$$

The global matrix equations are coupled and are solved under the following iterative procedures. At the beginning of the first iteration the values of (ψ_i).

Are taken to be 0 and the global equations (31) and (32) are solved for the nodal values of θ and ϕ. These nodal values (θi) and (ϕi) obtained are then used to solve the global equation (33) to obtain (ψ_i). In the second iteration these (ψ_i) values are obtained are used in (31) and (32) to calculate (θi) and (ϕi) and vice versa. The three equations are thus solved under iteration process until two consecutive iterations differ by a pre-assigned percentage.

The domain consists three horizontal levels and the solution for Ψ and θ at each level may be expressed in terms of the nodal values as follows.

In the horizontal strip $0 \leqslant y \leqslant c/3$:

$$\begin{aligned} \Psi &= \left(\Psi_1 \mathrm{N}_1^1 + \Psi_2 \mathrm{N}_2^1 + \Psi_7 \mathrm{N}_7^1\right) \mathrm{H}(1-\tau_1) \\ &= \Psi_1(1-4\mathrm{x}) + \Psi_2 4\left(\mathrm{x} - \frac{\mathrm{y}}{\mathrm{c}}\right) + \Psi_7\left(\frac{4\mathrm{y}}{\mathrm{c}}(1-\tau_1)\right) \qquad \left(0 \leqslant \mathrm{x} \leqslant \frac{1}{3}\right) \end{aligned}$$

$$\Psi = \left(\Psi_2 N_2^3 + \Psi_3 N_3^3 + \Psi_6 N_6^3\right) H(1-\tau_2) + \left(\Psi_2 N_2^2 + \Psi_7 N_7^2 + \Psi_6 N_6^2\right) H(1-\tau_3) \qquad \left(\frac{1}{3} \leqslant x \leqslant \frac{1}{3}\right)$$

$$= \left(\Psi_1 2(1-2x) + \Psi_3\left(4x - \frac{4y}{c} - 1\right) + \Psi_6\left(\frac{4y}{c}\right)\right) H(1-\tau_2) + \left(\Psi_2\left(1 - \frac{4y}{c}\right) + \Psi_7\left(1 + \frac{4y}{c} - 4x\right) + \Psi_6(4x-1)\right) H(1-\tau_3)$$

$$\Psi = \left(\Psi_3 N_3^5 + \Psi_4 N_4^5 + \Psi_5 N_5^5\right) H(1-\tau_3) + \left(\Psi_3 N_3^4 + \Psi_5 N_5^4 + \Psi_6 N_6^4\right) H(1-\tau_4) \qquad \left(\frac{2}{3} \leqslant x \leqslant 1\right)$$

$$= \left(\Psi_3(3-4x) + \Psi_4 2\left(2x - \frac{2y}{c} - 1\right) + \Psi_6\left(\frac{4y}{c} - 4x + 3\right)\right) H(1-\tau_3) + \Psi_3\left(1 - \frac{4y}{c}\right) + \Psi_5(4x-3) + \Psi_6\left(\frac{4y}{c}\right)\right) H(1-\tau_4)$$

Along the strip $c/3 \leqslant y \leqslant 2c/3$:

$$\Psi = \left(\Psi_7 N_7^6 + \Psi_6 N_6^6 + \Psi_8 N_8^6\right) H(1-\tau_2) \qquad \left(\frac{1}{3} \leqslant x \leqslant 1\right) + \left(\Psi_6 N_6^7 + \Psi_9 N_9^7 + \Psi_8 N_8^7\right) H(1-\tau_3) + \left(\Psi_6 N_6^8 + \Psi_5 N_5^8 + \Psi_9 N_9^8\right) H(1-\tau_4)$$

$$\Psi = \left(\Psi_7 2(1-2x) + \Psi_6(4x-3) + \Psi_8\left(\frac{4y}{c} - 1\right)\right) H(1-\tau_3) + \Psi_6\left(2\left(1 - \frac{2y}{c}\right) + \Psi_9\left(\frac{4y}{c} - 1\right) + \Psi_8\left(1 + \frac{4y}{c} - 4x\right)\right) H(1-\tau_4) + \Psi_6\left(4(1-x) + \Psi_5\left(4x - \frac{4y}{c} - 1\right) + \Psi_9 2\left(\frac{2y}{c} - 1\right)\right) H(1-\tau_5)$$

Along the strip $2c/3 \leqslant y \leqslant 1$:

$$\Psi = \left(\Psi_8 N_8^9 + \Psi_9 N_9^9 + \Psi_{10} N_{10}^9\right) H(1-\tau_6) \qquad \left(\frac{2}{3} \leqslant x \leqslant 1\right)$$

$$= \Psi_8\left(4(1-x) + \Psi_9 4\left(x - \frac{y}{c}\right) + \Psi_{10} 2\left(\frac{4y}{c} - 3\right)\right) H(1-\tau_6)$$

where $\tau_1 = 4x$, $\tau_2 = 2x$, $\tau_3 = 4x/3$, $\tau_4 = 4(x - y/c)$, $\tau_5 = 2(x - y/c)$, $\tau_6 = 4/3(x - y/c)$ and H represents the Heaviside function.

The expressions for θ are
In the horizontal strip $0 \leqslant y \leqslant c/3$:

$$\theta = \left(\theta_1(1-4x) + \theta_2 4\left(x - \frac{y}{c}\right) + \theta_7\left(\frac{4y}{c}\right)\right) H(1-\tau_1) \qquad \left(0 \leqslant x \leqslant \frac{1}{3}\right)$$

$$\theta = \left(\theta_2(2(1-2x) + \theta_3\left(4x - \frac{4y}{c} - 1\right) + \theta_6\left(\frac{4y}{c}\right)\right) H(1-\tau_2)$$
$$+\theta_2\left(1 - \frac{4y}{c}\right) + \theta_7\left(1 + \frac{4y}{c} - 4x\right) + \theta_6(4x-1))\, H(1-\tau_3) \qquad \left(\frac{1}{3} \leqslant x \leqslant \frac{2}{3}\right)$$

$$\theta = \theta_3(3-4x) + 2\theta_4\left(2x - \frac{2y}{c} - 1\right) + \theta_6\left(\frac{4y}{c} - 4x + 3\right)\right) H(1-\tau_3)$$
$$+\left(\theta_3\left(1 - \frac{4y}{c}\right) + \theta_5(4x-3) + \theta_6\left(\frac{4y}{c}\right)\right) H(1-\tau_4) \qquad \left(\frac{2}{3} \leqslant x \leqslant 1\right)$$

Along the strip $c/3 \leqslant y \leqslant 2c/3$:

$$\theta = \left(\theta_7(2(1-2x) + \theta_3(4x-3) + \theta_8\left(\frac{4y}{c} - 1\right)\right) H(1-\tau_3) \qquad \left(\frac{1}{3} \leqslant x \leqslant \frac{2}{3}\right)$$
$$+\left(\theta_6(2\left(1 - \frac{2y}{c}\right) + \theta_9\left(\frac{4y}{c} - 1\right) + \theta_8\left(1 + \frac{4y}{c} - 4x\right)\right) H(1-\tau_4)$$
$$+\left(\theta_6(4(1-x) + \theta_5\left(4x - \frac{4y}{c} - 1\right) + \theta_9 2\left(\frac{4y}{c} - 1\right)\right) H(1-\tau_5)$$

Along the strip $2c/3 \leqslant y \leqslant 1$:

$$\theta = \left(\theta_8 4(1-x) + \theta_9 4\left(x - \frac{y}{c}\right) + \theta_{10}\left(\frac{4y}{c} - 3\right)\right) H(1-\tau_6) \qquad \left(\frac{2}{3} \leqslant x \leqslant 1\right)$$

The expressions for ϕ are:

$$\phi = \left(\phi_1(1-4x) + \phi_2 4\left(x - \frac{y}{c}\right) + \phi_7\left(\frac{4y}{c}\right)\right) H(1-\tau_1) \qquad \left(0 \leqslant x \leqslant \frac{1}{3}\right)$$

$$\phi = \left(\phi_2\left(2(1-2x) + \phi_3\left(4x - \frac{4y}{c} - 1\right) + \phi_6\left(\frac{4y}{c}\right)\right) H(1-\tau_2)$$
$$+\phi_2\left(1 - \frac{4y}{c}\right) + \phi_7\left(1 + \frac{4y}{c} - 4x\right) + \phi_6(4x-1)\right) H(1-\tau_3) \qquad \left(\frac{1}{3} \leqslant x \leqslant \frac{2}{3}\right)$$

$$\phi = \phi_3(3-4x) + 2\phi_4\left(2x - \frac{2y}{c} - 1\right) + \phi_6\left(\frac{4y}{c} - 4x + 3\right) H(1-\tau_3)$$
$$+\left(\phi_3\left(1 - \frac{4y}{c}\right) + \phi_5(4x-3) + \phi_6\left(\frac{4y}{c}\right)\right) H(1-\tau_4) \qquad \left(\frac{2}{3} \leqslant x \leqslant 1\right)$$

Along the strip $c/3 \leqslant y \leqslant 2c/3$:

$$\phi = \left(\phi_7\left(2(1-2x) + \phi_6(4x-3) + \phi_8\left(\frac{4y}{c}-1\right)\right)\right) H(1-\tau_3) \qquad \left(\frac{1}{3} \leqslant x \leqslant \frac{2}{3}\right)$$
$$+\left(\phi_6\left(2\left(1-\frac{2y}{c}\right) + \phi_9\left(\frac{4y}{c}-1\right) + \phi_8\left(1+\frac{4y}{c}-4x\right)\right)\right) H(1-\tau_4)$$
$$+\left(\phi_6\left(4\left(1-x\right) + \phi_5\left(4x-\frac{4y}{c}-1\right) + \phi_9 2\left(\frac{4y}{c}-1\right)\right)\right) H(1-\tau_5)$$

Along the strip $2c/3 \leqslant y \leqslant 1$:

$$\phi = \left(\phi_8 4(1-x) + \phi_9 4\left(x-\frac{y}{c}\right) + \phi_{10}\left(\frac{4y}{c}-3\right)\right) H(1-\tau_6) \qquad \left(\frac{2}{3} \leqslant x \leqslant 1\right)$$

The dimensionless Nusselt numbers (Nu) and Sherwood Numbers (Sh) on the non-insulated boundary walls of the rectangular duct are calculated using the formula:

$$Nu = \left(\frac{\partial \theta}{\partial x}\right)_{x=1 \text{ and}} \quad Sh = \left(\frac{\partial \phi}{\partial x}\right)_{x=1}$$

Nusselt Number on the side wall $x = 1$ in different regions are:

$Nu_1 = 2 - 4\theta_3$ $(0 \leqslant y \leqslant c/3)$
$Nu_2 = 2 - 4\theta_6$ $(c/3 \leqslant y \leqslant 2c/3)$
$Nu_3 = 2 - 4\theta_8$ $(2c/3 \leqslant y \leqslant c)$

Sherwood Number on the side wall $x = 1$ in different regions are:

$Sh_1 = 2 - 4\phi_3$ $(0 \leqslant y \leqslant c/3)$
$Sh_2 = 2 - 4\phi_6$ $(c/3 \leqslant y \leqslant 2c/3)$
$Sh_3 = 2 - 4\phi_8$ $(2c/3 \leqslant y \leqslant c)$

5. Comparison

In this analysis, it should be mentioned that the results obtained herein are compared with the results of Shanthi *et al.* (2011) in the absence of $Q_1 = 0$ and also compared with the results of Badruddin *et al.* (2006) in the absence of mass transfer ($N = 0$) and chemical reaction, the results are good agreement.

6. Results and discussion

The equations governing momentum, energy and diffusion transfer are solved by using Galerkin Finite Element Analysis with triangular elements and bi-linear shape functions.

The temperature and concentration distributions are exhibited in Figures 2-17 for different variations of So, N, γ and α_1 at different vertical and horizontal levels. Figures 2-5 represents the variation of with Soret parameter So (0.5, 1, −1.5, −1 and −0.5). At the vertical levels $x = 1/3$ and 2/3 the actual temperature reduces with $So > 0$ and enhances with $|So|$ (Figures 4 and 5). At the horizontal levels an increase in $So > 0$ reduces the actual temperature at $y = c/3$ level and enhances at $y = 2c/3$ level, while it enhances at $y = c/3$ level and reduces at $y = 2c/3$ level with increase in $|So|$ (Figures 2 and 3). The variation of θ with buoyancy ratio N (1, 2, −0.5 and −0.8) is shown in Figures 6-9 at different levels. It is found that the molecular buoyancy force dominates

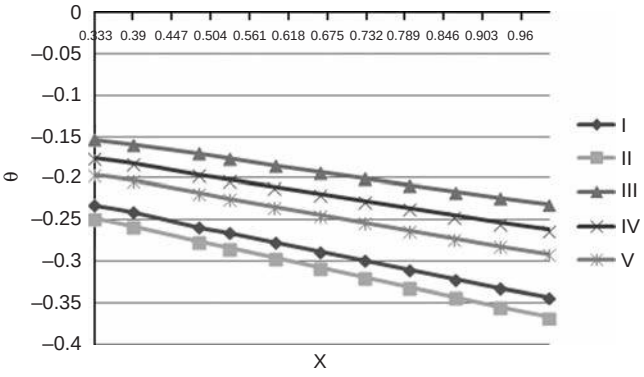

Figure 3.
Variation of θ with So at y = 2c/3 level

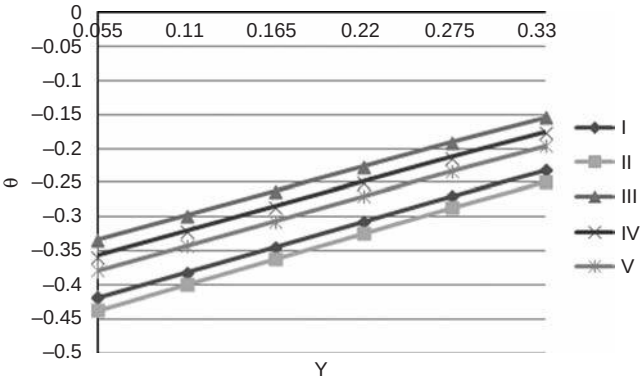

Figure 4.
Variation of θ with So at x = 1/3 level

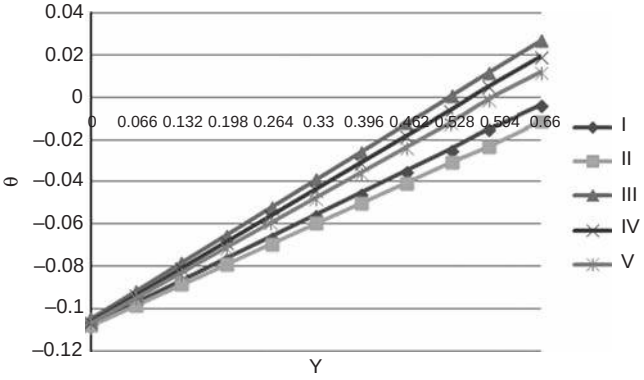

Figure 5.
Variation of θ with So at x = 2/3 level

the thermal buoyancy force the actual temperature reduces at all vertical levels and horizontal level y = c/3 and enhances at higher vertical level y = 2c/3 when the buoyancy forces act in the same direction and for the forces acting in the opposite directions the actual temperature enhances at all vertical levels and at y = c/3 while depreciates at y = 2c/3 level. The effect of chemical reaction (0.5, 1.5, 2, −0.5, −1.5 and −2.5)

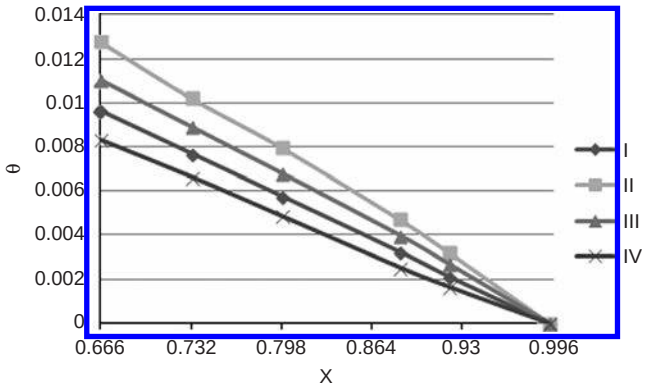

Figure 6.
Variation of θ with N at y = c/3 level

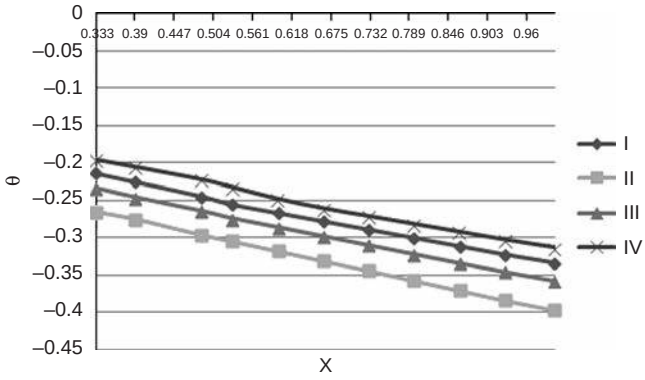

Figure 7.
Variation of θ with N at y = 2c/3 level

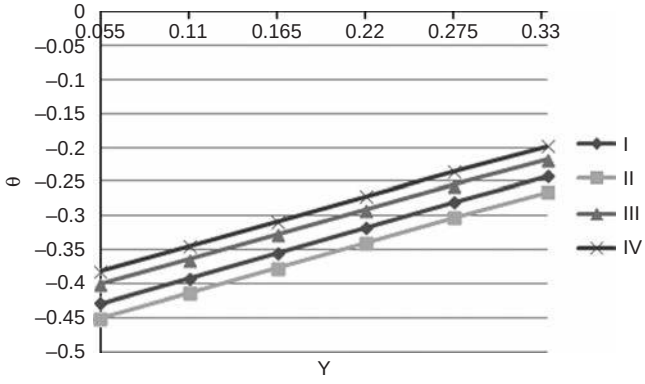

Figure 8.
Variation of θ with N at x = 1/3 level

on is shown in Figures 10-13 at all levels. It is found that the actual temperature reduces in the degenerating chemical reaction case and enhances in the generating chemical reaction case at both the horizontal levels and in the generating chemical reaction case the actual temperature enhances at both the horizontal levels. At x = 1/3 level the actual temperature enhances both generating and degenerating chemical reaction. At higher

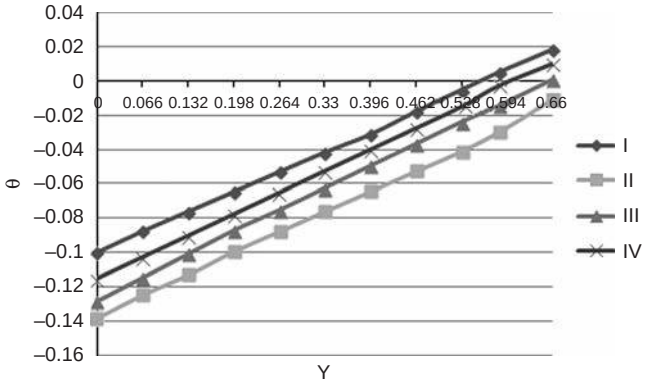

Figure 9.
Variation of θ with N at x = 2/3 level

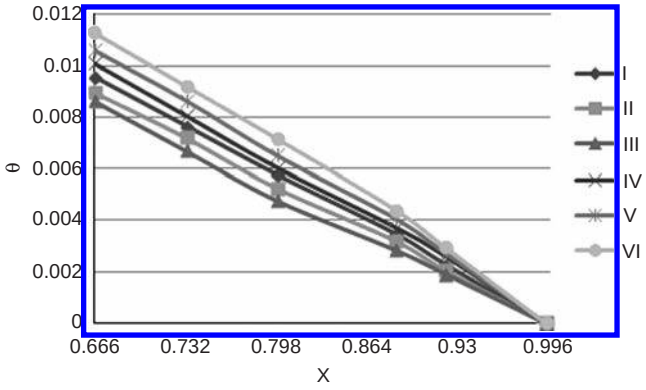

Figure 10.
Variation of θ with γ at y = c/3 level

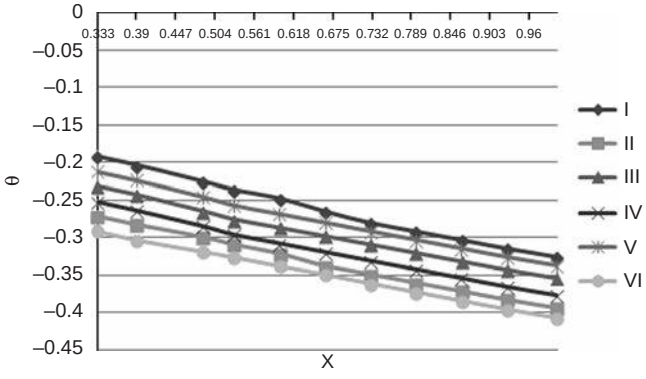

Figure 11.
Variation of θ with γ at y = 2c/3 level

vertical level x = 2/3 the actual temperature enhances in the degenerating case except in the horizontal strip (0.528, 0.66) and in the generating case it depreciates except in the region (0.462, 0.66) (Figure 13). The effect of inclination of the magnetic field ($\pi/3$,$\pi/2$,$\pi/4$ and π) on θ is shown in Figures 14-17. It is found that an increase in the inclination $\alpha_1 \leqslant \pi/2$ results an enhancement in the actual temperature and for higher $\alpha_1 \geqslant \pi_1$ we notice an enhancement in the actual temperature at all the horizontal and vertical levels.

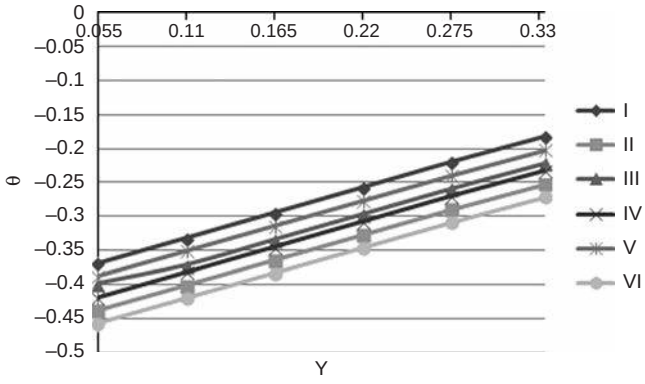

Figure 12.
Variation of θ with γ at x = 1/3 level

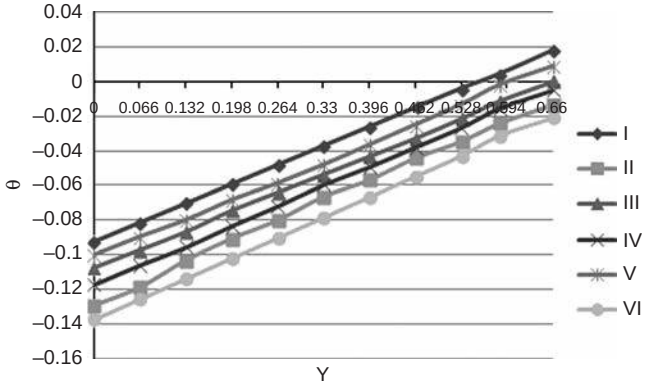

Figure 13.
Variation of θ with γ at x = 2/3 level

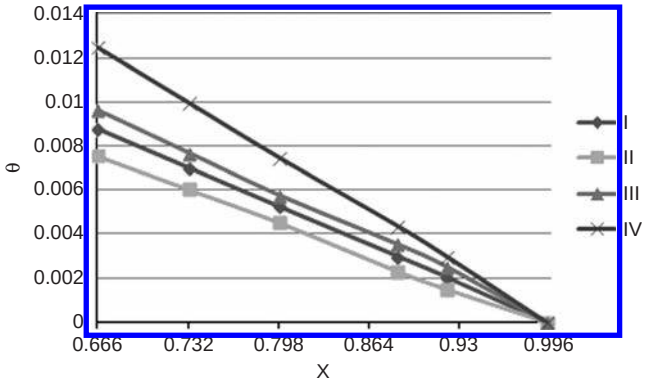

Figure 14.
Variation of θ with α_1 at y = c/3 level

The non-dimensional concentration is shown in Figures 18-33 for different parametric variations at different horizontal and vertical levels. We follow the convention that the non-dimensional concentration is positive or negative according as the actual concentration is greater or lesser than C. Figures 18-21 represent the effect of So (0.5, 1, −1.5, −1 and −0.5) on C. It is found that the actual concentration depreciates with So > 0

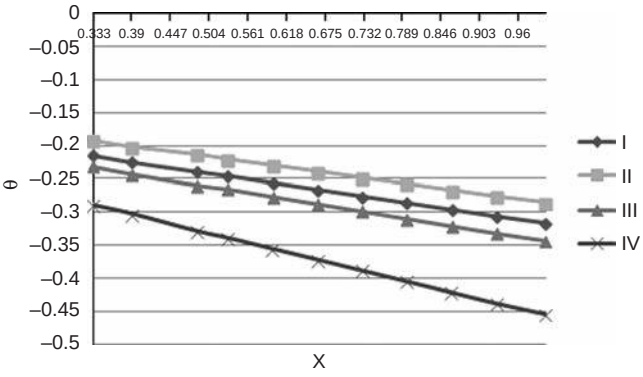

Figure 15.
Variation of θ with α_1 at $y = 2c/3$ level

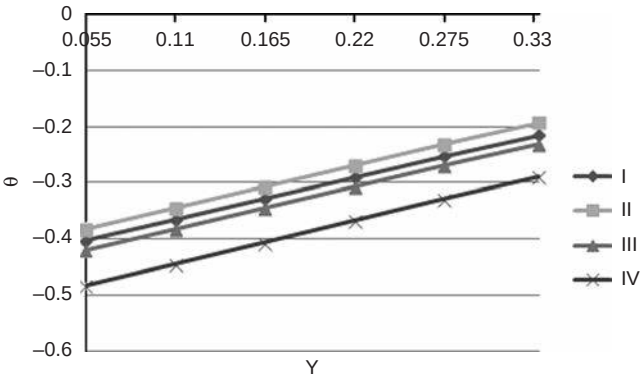

Figure 16.
Variation of θ with α_1 at $x = 1/3$ level

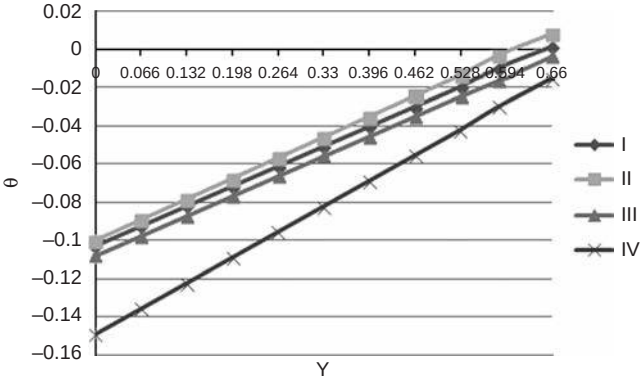

Figure 17.
Variation of θ with α_1 at $x = 2/3$ level

and enhances with $So < 0$ at $y = c/3$ level and $x = 1/3$ level and at $y = 2c/3$ level it enhances with $So > 0$ and depreciates with $So < 0$ (Figures 18 and 19). At the higher vertical level $x = 2/3$ an increase in $So > 0$ reduces the actual concentration in the region (0, 0.33) and enhances in the region (0.396, 0.66) while it increase for $So < 0$ we notice an enhancement in the actual concentration in the region (0, 0.33) and depreciates in the

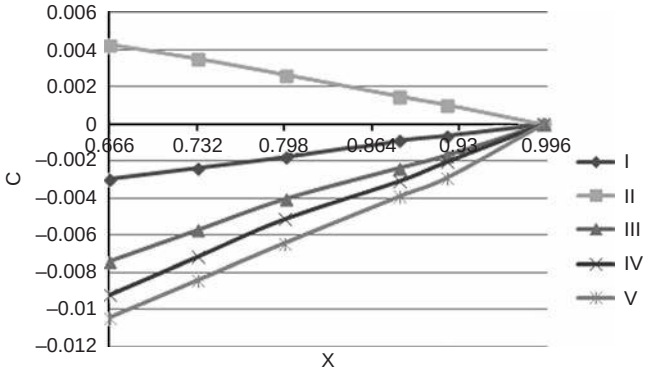

Figure 18.
Variation of C with So at y = c/3 level

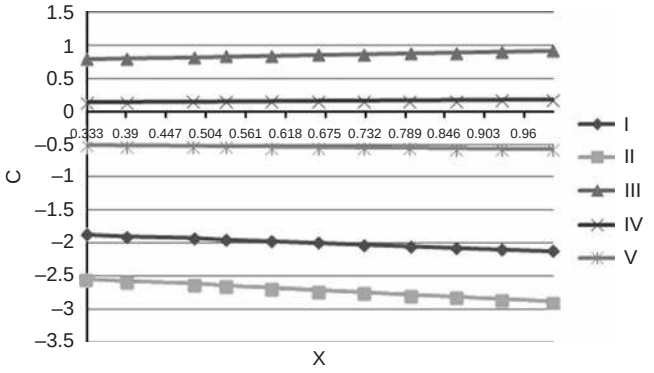

Figure 19.
Variation of C with So at y = 2c/3 level

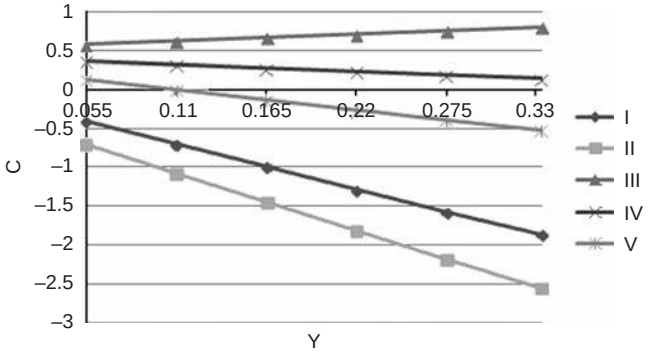

Figure 20.
Variation of C with So at x = 1/3 level

region (0.396, 0.66) (Figure 21). The effect of buoyancy ratio N (1,2,−0.5 and −0.8) on C is shown in Figures 22-25. It is found that at both the horizontal levels and vertical level x = 1/3 the actual concentration enhances when buoyancy forces act in the same directions and for the forces acting in opposite direction the actual concentration depreciates at y = c/3 and x = 1/3 levels and enhances at y = 2c/3 level (Figures 22-24) at the higher vertical level x = 2/3 the actual concentration enhances in the horizontal strip (0, 0.33) and reduces in the strip (0.396, 0.66) while a reversed effect is observed for N < 0

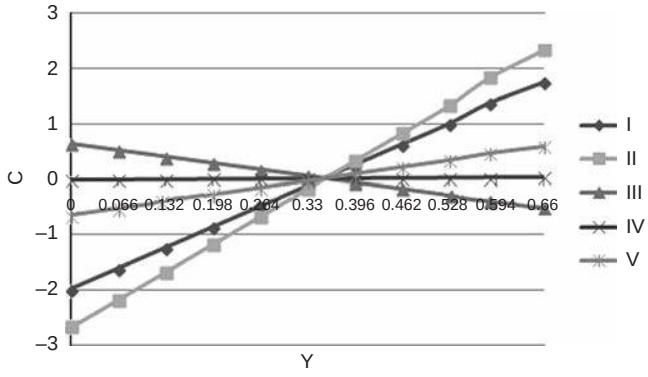

Figure 21.
Variation of C with So at x = 2/3 level

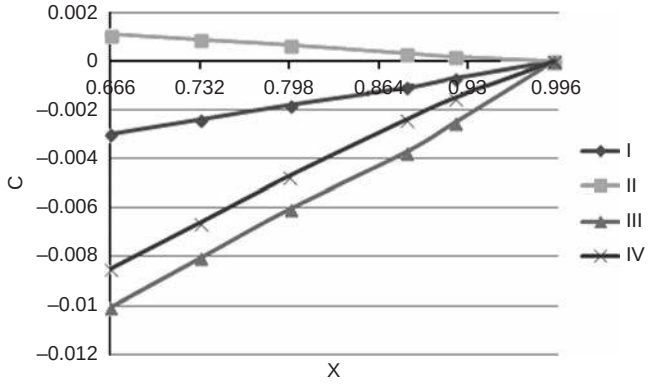

Figure 22.
Variation of C with N at y = c/3 level

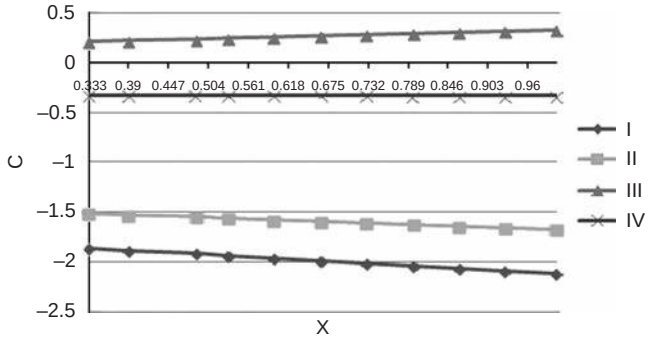

Figure 23.
Variation of C with N at y = 2c/3 level

(Figure 25). The effect of chemical reaction parameter γ (0.5,1.5,2,−0.5,−1.5 and −2.5) on C is shown in Figures 26-29. It is found that at both the horizontal levels and vertical level x = 1/3 the actual concentration depreciates in the degenerating chemical reaction case and enhances in the generating chemical reaction case at higher vertical level x = 2/3. The actual concentration depreciates in the degenerating chemical reaction case and in the generating chemical reaction case it enhances in the horizontal strip (0, 0.396) and

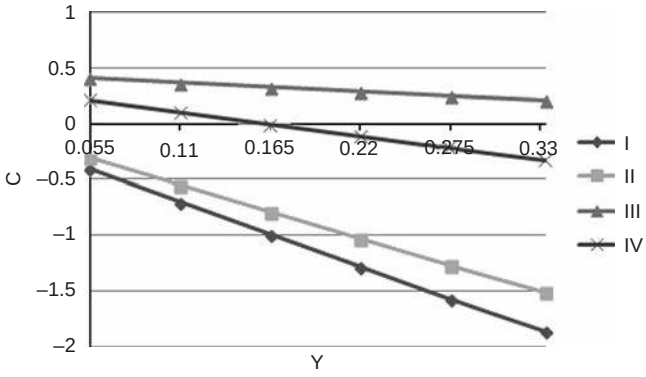

Figure 24.
Variation of C with N at x = 1/3 level

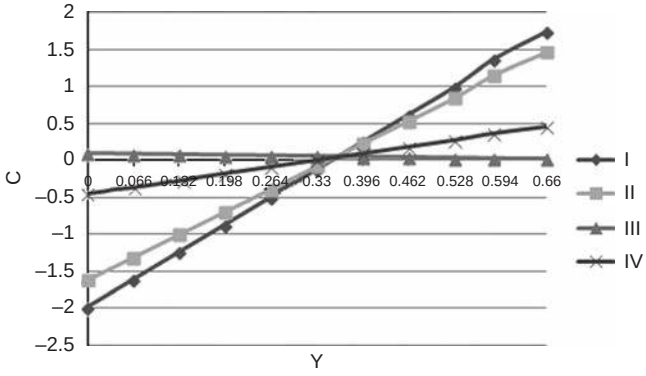

Figure 25.
Variation of C with N at x = 2/3 level

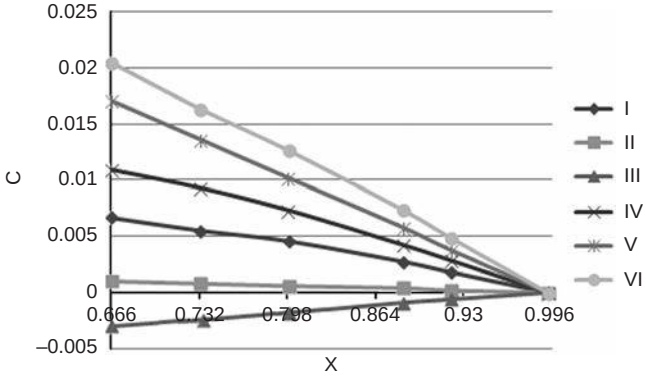

Figure 26.
Variation of C with γ at y = c/3 level

depreciates in the strip (0.462, 0.66) (Figure 29). The effect of inclination of the magnetic field α_1 ($\pi/3$,$\pi/2$,$\pi/4$ and π) on C is shown in Figures 30-33. It is found that an increase in the inclination $\alpha_1 \leqslant \pi/2$ results in a depreciation in the actual concentration and for higher $\alpha_1 \geqslant \pi$ we notice an enhancement in the actual concentration at all the horizontal and vertical levels.

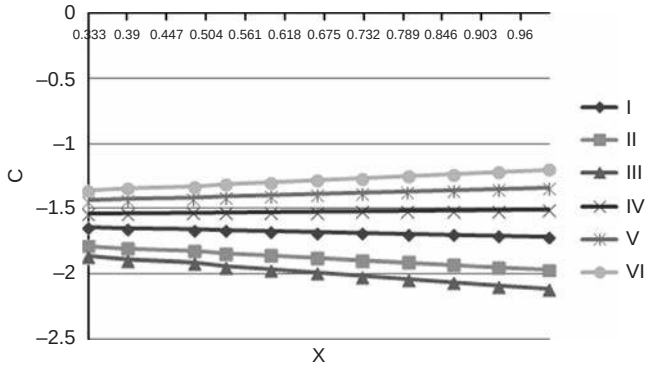

Figure 27.
Variation of C with γ at y = 2c/3 level

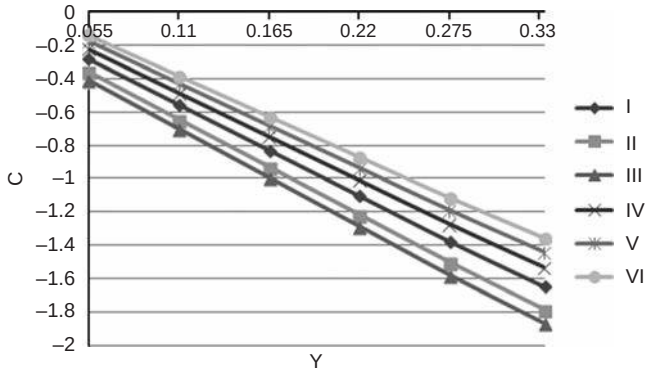

Figure 28.
Variation of C with γ at x = 1/3 level

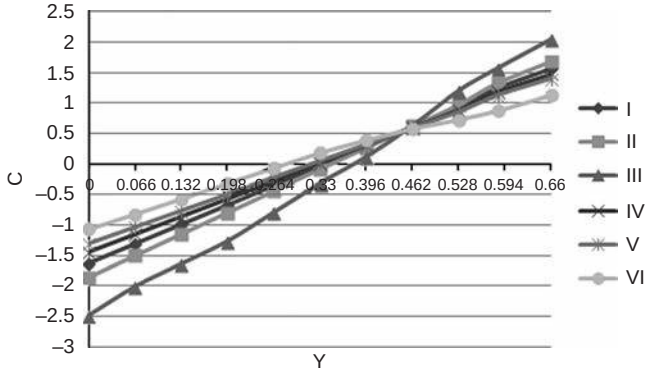

Figure 29.
Variation of C with γ at x = 2/3 level

The rate of heat transfer on x = 1 is shown in Tables I-IV for different parametric values. The effect of Soret parameter So on Nu is shown in the Table I. It is observed that the rate of heat transfer enhances with So > 0 and depreciates with |So| at all the three quadrants. Table II represents the variation of Nu with buoyancy ratio N and Dufour effect Du. Then the molecular buoyancy force dominates over the thermal buoyancy force the rate of heat transfer enhances at all the quadrants when thermal buoyancy forces act in the same direction and for the forces acting in opposite

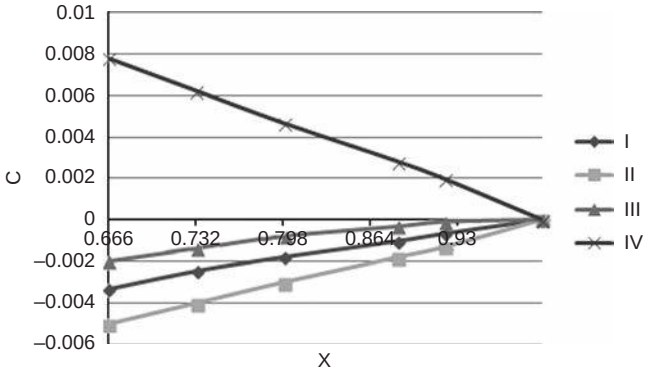

Figure 30.
Variation of C with α_1 at $y = c/3$ level

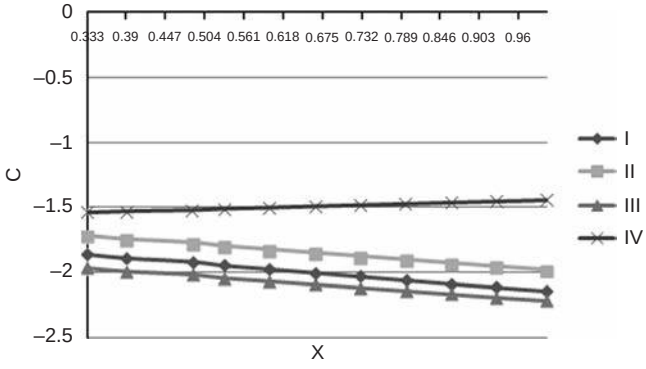

Figure 31.
Variation of C with α_1 at $y = 2c/3$ level

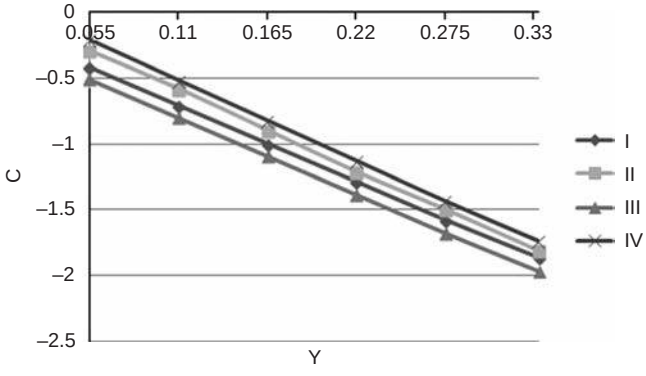

Figure 32.
Variation of C with α_1 at $x = 1/3$ level

directions |Nu| depreciates at all quadrants. The effect of Dufour effect on Nu is shown in Table II. It is found that the Nu experiences an enhancement at all the three quadrants with increase in Du. The effect of chemical reaction on Nu is shown in Table III. It is found that an increase in chemical reaction parameter $\gamma < 1.5$ enhances Nu and depreciates with higher $\gamma > 2.5$ at lower and middle quadrants while at the upper quadrant |Nu| reduces with $\gamma < 1.5$ and enhances with $\gamma > 2.5$. In the generating chemical reaction case the Nusselt number Nu enhances at the lower and middle

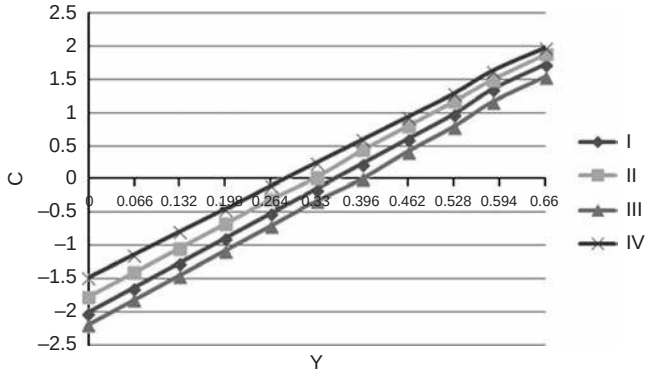

Figure 33.
Variation of C with α_1 at x = 2/3 level

	So	0.5	1	−1.5	−1	−0.5
Table I. Nusselt number at x = 1 level	Nu1	2.431364	2.431528	2.419068	2.423688	2.427352
	Nu2	2.223104	2.238738	2.155943	2.173322	2.190341
	Nu3	2.014842	2.045947	1.892819	1.922957	1.95333

	N	1	2	−0.5	−0.8	1	1	1
	Du	0.01	0.01	0.01	0.01	0.03	0.05	0.07
Table II. Nusselt number at x = 1 level	Nu1	2.432	2.497	2.514	2.462	5.069	5.072	5.078
	Nu2	2.223	2.264	2.238	2.211	3.124	3.180	3.131
	Nu3	2.015	2.031	1.962	1.961	2.721	2.712	2.817

	γ	0.5	1.5	2.5	−0.5	−1.5	−2.5
Table III. Nusselt number at x = 1 level	Nu1	2.431	2.438	2.424	2.457	2.464	2.470
	Nu2	2.223	2.225	2.221	2.231	2.232	2.233
	Nu3	2.015	2.012	2.018	2.004	2.003	1.997

	Rad	0.05	0.5	1.5	2.5	0.05	0.05	0.05
	α_1	π/4	π/4	π/4	π/4	π/3	π/2	π
Table IV. Nusselt number at x = 1 level	Nu1	2.431	2.558	2.747	2.863	2.411	2.401	2.597
	Nu2	2.223	2.252	2.270	2.264	2.204	2.185	2.329
	Nu3	2.015	1.947	1.794	1.666	1.996	1.969	2.062

quadrants and depreciates at the upper quadrant. The effect of inclined magnetic field α_1 and thermal radiation parameter Rad on Nu is shown in Table IV. It is found that the rate of heat transfer reduces with increase in inclination $\alpha_1 \leqslant \pi/2$ and enhances with higher $\alpha_1 \geqslant \pi$. An increase in the thermal radiation parameter Rad results in an enhancement in the rate of heat transfer at all the three quadrants (Table IV).

The rate of mass transfer (Sh) is exhibited in Table V-VIII for different parametric values. Table V represents Sh with Soret parameter So. It is noticed that the rate of mass transfer at the lower and middle quadrants enhances with $So > 0$ and reduces with $|So|$. At the upper quadrants $|Sh|$ reduces with $So > 0$ and enhances with $|So|$. Table V represents the variation of Sh with inclination α_1. It is found that $|Sh|$ reduces with $\alpha_1 \leqslant \pi/2$ and reduces with $\alpha_1 \geqslant \pi/2$ while at the upper quadrants it reduces with $\alpha_1 \leqslant \pi/2$ and enhances with $\alpha_1 \geqslant \pi$. The variation of Sh with buoyancy ratio N is shown in Table VI. It is found that the rate of mass transfer reduces with $N > 0$ and enhances with $|N|$. An increase in the Dufour parameter Du results in an enhancement $|Sh|$ at all the three quadrants (Table VI). The effect of chemical reaction on Sh is shown in Table VII. The rate of mass transfer at the lower and middle quadrants reduces with $\gamma \leqslant 1.5$ and enhances with $\gamma \geqslant 2.5$ while at the upper quadrant it enhances with γ. In the generating chemical reaction case the rate of mass transfer at all the quadrants depreciates with γ. The effect of thermal radiation on Sh is shown in Table VIII. It is

So	0.5	1	−1.5	−1	−0.5	0.5	0.5	0.5
α_1	π/4	π/4	π/4	π/4	π/4	π/3	π/2	π
Sh1	9.956	12.698	−0.526	2.023	4.618	10.036	9.899	8.737
Sh2	2.498	2.676	1.762	1.941	2.127	2.498	2.498	2.498
Sh3	−4.96	−7.35	4.049	1.859	−0.364	−4.959	−4.959	−4.95

Table V. Sherwood number at x = 1 level

N	1	2	−0.5	−0.8	1	1	1
Du	0.01	0.01	0.01	0.01	0.03	0.05	0.07
Sh1	9.956	8.492	1.625	3.805	8.421	8.401	8.368
Sh2	2.498	2.317	1.776	2.006	2.453	2.168	2.167
Sh3	−4.959	−3.857	1.926	0.207	1.485	−4.559	−4.05

Table VI. Sherwood number Sh at x = 1 level

γ	0.5	1.5	2	2.5	−0.5	−1.5	−2.5
Sh1	9.956	9.430	9.956	10.542	7.795	7.180	6.661
Sh2	2.498	2.359	2.498	2.656	1.949	1.803	1.684
Sh3	−4.959	−4.710	−4.498	−5.230	−3.898	−3.575	−3.292

Table VII. Sherwood number Sh at x = 1 level

Rad	0.05	0.5	1.5	2.5
Sh1	9.956	10.049	10.172	10.245
Sh2	2.498	2.539	2.575	2.587
Sh2	−4.959	−4.971	−5.022	−5.071

Table VIII. Sherwood number Sh at x = 1 level

observed that higher the thermal radiative heat flux larger the rate of mass transfer at all the three quadrants.

7. Conclusions

(1) At the vertical levels, the temperature reduces with $|So|$. At the horizontal levels, an increase in $So > 0$ reduces the actual temperature.

(2) An increase in the inclination $\alpha_1 \leqslant \pi/2$ results an enhancement in the actual temperature and for higher inclination $\alpha_1 \geqslant \pi$ we notice an enhancement in the actual temperature at all the horizontal and vertical levels.

(3) At the higher vertical level $x = 2/3$, an increase in $So > 0$ reduces the actual concentration in the region (0, 0.33) and enhances in the region (0.396, 0.66) while it increase for $So < 0$ we notice an enhancement in the actual concentration in the region (0, 0.33) and depreciates in the region (0.396, 0.66).

(4) An increase in the inclination $\alpha_1 \leqslant \pi/2$ results in a depreciation in the actual concentration and for higher $\alpha_1 \geqslant \pi$ we notice an enhancement in the actual concentration at all the horizontal and vertical levels.

(5) The rate of heat transfer enhances with $So > 0$ and depreciates with $|So|$ at all the three quadrants. The rate of heat transfer experiences an enhancement at all the three quadrants with increase in Du.

(6) An increase in the thermal radiation parameter Rad results in an enhancement in the rate of heat transfer at all the three quadrants. The rate of heat transfer reduces with increase in inclination $\alpha_1 \leqslant \pi/2$ and enhances with higher $\alpha_1 \geqslant \pi$.

(7) $|Sh|$ reduces with $\alpha_1 \leqslant \pi/2$ and reduces with $\alpha_1 \geqslant \pi/2$ while at the upper quadrants it reduces with $\alpha_1 \leqslant \pi/2$ and enhances with $\alpha_1 \geqslant \pi$. An increase in the Dufour parameter Du results in an enhancement $|Sh|$ at all the three quadrants. We notice that higher the thermal radiative heat flux larger the rate of mass transfer at all the three quadrants.

References

Al-Farhany, K. and Turan, A. (2012), "Numerical study of double diffusive natural convective heat and mass transfer in an inclined rectangular cavity filled with porous medium", *International Communications in Heat and Mass Transfer*, Vol. 39, pp. 174-181.

Badruddin, I.A., Zainal, Z.A., Aswatha, N. and Seetharamu, K.N. (2006), "Heat transfer in porous cavity under the influence of radiation and viscous dissipation", *International Communication in Heat and Mass Transfer*, Vol. 33, pp. 491-499.

Bankvall, C.G. (1972), "Natural convective heat transfer in a insulated structures", *Lundinst. Tech. Report*, Vol. 38, pp. 1-149.

Bankvall, C.G. (1973), "Heat transfer in fibrous material", *Journal of Test E*, Vol. 3, pp. 235-243.

Bankvall, C.G. (1974), "Natural convective in vertical permeable space", *Warme and Staffubertragung*, Vol. 7, pp. 22-30.

Bathe, K.J. (1996), *Finite Element Procedures*, Prentice-Hall, Upper Saddle River, NJ.

Burns, P.J., Chow, L.C and Chen, S. (1926), "Heat transfer in rectangular geometry in a porous medium", *International Journal of Heat and Mass Transfer*, Vol. 20, pp. 919-926.

Chamkha, A.J. and Al-Naser, H. (2002), "Hydromagnetic double-diffusive convection in a rectangular enclosure with uniform side heat and mass fluxes and opposing temperature and concentration gradients", *International Journal of Thermal Sciences*, Vol. 41, pp. 936-948.

Cheng, C.-Y. (2011), "Soret and Dufour effects on natural convection boundary layer flow over a vertical cone in a porous medium with constant wall heat and mass fluxes", *International Communications in Heat and Mass Transfer*, Vol. 38, pp. 44-48.

Cheng, K.S. and Hi, J.R. (1987), "Steady two-dimensional natural convection in rectangular enclosures with differently heated walls", *Transaction of the American Society of Mechanical Engineers*, Vol. 109, p. 400.

Chiu, H.-C., Jang, J.-H. and Wei-Monyan (2007), "Mixed convection heat transfer in horizontal rectangular ducts with radiation effects", *International Journal of Heat and Mass Transfer*, Vol. 50, pp. 2874-2882.

Chittibabu, D., Prasada Rao, D.R.V. and Krishna, D.V. (2006), "Convection flow through a porous medium in ducts", *Acta Ciencia Indica*, Vol. 30 No. 2, pp. 635-642.

Dulal, P. and Hiranmoy, M. (2011), "Effects of Soret Dufour, chemical reaction and thermal radiation on MHD non-Darcy unsteady mixed convective heat and mass transfer over a stretching sheet", *Communication in Nonlinear Science and Numerical Simulation*, Vol. 16, pp. 1942-1958.

Gnaneswara Reddy, M. and Bhaskar Reddy, N. (2010), "Soret and Dufour effects on steady MHD free convection flow past a semi-infinite moving vertical plate in a porous medium with viscous dissipation", *International Journal of Applied Mathematics and Mechanics*, Vol. 6 No. 1, pp. 1-12.

Hyun, J.M. and Lee, J.W. (1990), "Double-diffusive convection in a rectangle with cooperating horizontal gradients of temperature and concentration gradients", *International Journal of Heat and Mass Transfer*, Vol. 33, pp. 1605-1617.

Ibrahim, F.S., Elaiw, A.M. and Bakr, A.A. (2008), "Effect of chemical reaction radiation absorption on the unsteady MHD free convection flow past a semi-infinite vertical permeable moving plate with heat source and suction", *Communication in Nonlinear Science and Numerical Simulation*, Vol. 13, pp. 1056-1066.

Lee, J.W. and Hyun, J.M. (1990), "Double-diffusive convection in a rectangle with opposing horizontal and concentration gradients", *International Journal of Heat and Mass Transfer*, Vol. 33, pp. 1619-1632.

Mahapatra, T.R., Dulal, P. and Mondal, S. (2012), "Mixed convection flow in an inclined enclosure under magnetic field with thermal radiation and heat generation", *International Communications in Heat and Mass Transfer*, Vol. 41, pp. 47-56.

Makinde, O.D. (2005), "Free convection flow with thermal radiation and mass transfer past a moving vertical porous plate", *International Communications in Heat and Mass Transfer*, Vol. 32, pp. 1411-1419.

Nagaradhika, V., Gayathri, Y., Prasada Rao, D.R.V. and Ajay, V. (2011), "Convective heat transfer in a rectangular cavity under the influence of radiation, viscous dissipation and temperature gradient dependent heat source", *International Journal of Electrical, Electronics and Computing Technology*, Vol. 2 No. 4, pp. 109-117.

Rao, J.A. and Shivaiah, S. (2011), "Chemical reaction effects on unsteady MHD flow past semi-infinite vertical porous plate with viscous dissipation", *Applied Mathematics and Mechanics (English Edition)*, Vol. 32 No. 8, pp. 1065-1078.

Reddy, J.N. (1985), *An Introduction to the Finite Element Method*, McGraw-Hill, NewYork, NY.

Revnic, C., Grosan, T., Pop, I. and Ingham, D.B. (2011), "Magnetic field effect on the unsteady free convection flow in a square cavity filled with a porous medium with a constant heat generation", *International Journal of Heat and Mass Transfer*, Vol. 54, pp. 1734-1742.

Ribando, R.J. and Torrance, K.E. (1976), "Natural convection in a porous medium effects of confinement, variable permeability and thermal boundary conditions", *Trans of American Society of Mechanical Engineers*, Vol. 98, pp. 42-48.

Rubin, A. and Schweitzer, S. (1972), "Heat transfer in porous media with phase change", *International Journal of Heat and Mass Transfer*, Vol. 15, pp. 43-59.

Seki, N., Fukusako, S. and Inaba, H. (1981), "Heat transfer in a confined rectangular cavity packed with porous media", *International Journal of Heat and Mass Transfer*, Vol. 21, pp. 985-989.

Shanthi, G., Jafarunissa, S. and Prasada Rao, D.R.V. (2011), "Finite element analysis of convective heat and mass transfer flow of a viscous electrically conducting fluid through a porous medium in a rectangular cavity with dissipation", *International Journal of Electrical, Electronics and Computing Technology*, Vol. 2 No. 4, pp. 29-34.

Shehadeh, F.G. and Duwairi, H.M. (2009), "MHD natural convection in porous media-filled enclosures", *Applied Mathematics and Mechanics (English Edition)*, Vol. 30 No. 9, pp. 1113-1120.

Sivaiah, S. (2004), "Thermo-Diffusion effects on convective heat and mass transfer through a porous medium in Ducts", PhD thesis, Sri Krishnadevaraya University, Anantapur.

Srinivas, S., Subramanyam Reddy, A. and Ramamohan, T.R. (2012), "A study on thermal-diffusion and diffusion-thermo effects in a two-dimensional viscous flow between slowly expanding or contracting walls with peak permeability", *International Journal of Heat and Mass Transfer*, Vol. 55, pp. 3008-3020.

Tai, B.-C. and Ming, I.-C. (2010), "Soret and Dufour effects on free convection flow of non Newtonian fluids along a vertical plate embedded in a porous medium with thermal radiation", *International Communications in Heat and Mass Transfer*, Vol. 37, pp. 480-483.

Verschoor, J.D. and Greebler, P. (1952), "Heat transfer by gas conduction and radiation in fibrous insulation transfer", *Trans of American Society of Mechanical Engineers*, pp. 961-968.

Corresponding author
Professor Ali J. Chamkha can be contacted at: achamkha@yahoo.com